

## Structural, FTIR and ac conductivity studies of NaMeO<sub>3</sub> (Me ≡ Nb, Ta) ceramics

Sumit K. Roy<sup>1</sup>, S.N. Singh<sup>2</sup>, K. Kumar<sup>3</sup> and K. Prasad<sup>\*4</sup>

<sup>1</sup>Department of Physics, St. Xavier's College, Ranchi – 834 001, India

<sup>2</sup>University Department of Physics, Ranchi University, Ranchi – 834 008, India

<sup>3</sup>Refractory Division, RDCIS, SAIL, Ranchi – 834 002, India

<sup>4</sup>University Department of Physics, T. M. Bhagalpur University, Bhagalpur – 812 007, India

(Received May 19, 2013, Revised July 10, 2013, Accepted August 6, 2013)

**Abstract.** Lead-free complex perovskite ceramics NaMeO<sub>3</sub> (Me ≡ Nb, Ta) were synthesized using conventional solid state reaction technique and characterized by structural, FTIR and electrical (dielectric and ac conductivity) studies. The crystal symmetry, space group and unit cell dimensions were determined from the experimental results using FullProf software. XRD analysis of the compound indicated the formation of single-phase orthorhombic structure with the space group *Pmmm* (47). Dielectric studies showed the diffuse phase transition at 394°C for NaNbO<sub>3</sub> and 430°C for NaTaO<sub>3</sub>. Ac conductivity in both the compounds follows Jonscher's power law.

**Keywords:** NaNbO<sub>3</sub>; NaTaO<sub>3</sub>; perovskite; dielectric properties; lead-free; electroceramic

---

### 1. Introduction

Ceramics with ABO<sub>3</sub>-type of structure have been widely used in various electronic and microelectronic devices such as capacitors, piezoelectric transducers, pyroelectric detectors/sensors, memory devices, microwave tunable devices, electrorestrictive actuators, SAW substrates, MEMS, *etc.* It has been observed that materials used for most of these applications are made from lead bearing compounds such as lead titanate, lead zirconate titanate, lead magnesium niobates, *etc.* In recent years, continuous efforts are being made worldwide to improve the performance characteristics of lead-free ABO<sub>3</sub>-type materials suitable for practical applications (Seo *et al.* 2013, Du *et al.* 2013a, Du *et al.* 2013b, Vendrell *et al.* 2013b, Bhagat *et al.* 2013, AmarNath and Prasad 2012, Kumari *et al.* 2011, Eichel and Kungl 2010, Damjanovic *et al.* 2010, Panda 2009, Rödel *et al.* 2009, Wunderlich 2009, ShROUT and Zhang 2007, Takenaka and Nagata 2005). Among them, NaNbO<sub>3</sub> and NaTaO<sub>3</sub> are well-known perovskite oxides and are considered to be feasible alternatives to commercial Pb-containing piezoceramics (Koruza *et al.* 2010, Hsiao *et al.* 2007, Chen *et al.* 2005, Reznitchenko *et al.* 2001, Kennedy *et al.* 1999). Further, the studies of dielectric properties and electrical conductivity in such compounds are very important since the associated physical properties are dependent on the nature and magnitude of conductivity in these materials.

---

\*Corresponding author, Ph.D., E-mail: [k.prasad65@gmail.com](mailto:k.prasad65@gmail.com); [k\\_prasad65@yahoo.co.in](mailto:k_prasad65@yahoo.co.in)

Accordingly, in the present work, the structural (X-ray and its Rietveld analysis), FTIR, dielectric and ac conductivity properties of perovskite  $\text{NaNbO}_3$  and  $\text{NaTaO}_3$  (abbreviated hereafter NN and NT, respectively) ceramics have been presented.

## 2. Materials and methods

The polycrystalline samples of  $\text{NaMeO}_3$  ( $\text{Me} \equiv \text{Nb, Ta}$ ) were prepared by the conventional solid-state reaction technique using the thermochemical reaction:  $\text{Na}_2\text{CO}_3 + \text{Me}_2\text{O}_5 \xrightarrow{\Delta} \text{NaMeO}_3 + \uparrow \text{CO}_2(\text{g})$ . High purity (>99.9%) carbonates/oxides of  $\text{Na}_2\text{CO}_3$  (Merck, Germany) and  $\text{Nb}_2\text{O}_5$  (Hi media, India) /  $\text{Ta}_2\text{O}_5$  (Aldrich, USA) were mixed in proper stoichiometric quantities. Wet mixing was carried out with acetone as the medium for homogeneous mixing. Grinding was performed using a ball milling apparatus for about 1 h. Well-mixed powders were then calcined at  $850^\circ\text{C}$  and  $1080^\circ\text{C}$  for 4 h, respectively for NN and NT. The as-calcined powders were compacted into thin (~1.5 mm) cylindrical disks with an applied uniaxial pressure of 650 MPa. The pellets were then sintered in air atmosphere at  $900^\circ\text{C}$  for NN and at  $1100^\circ\text{C}$  for NT in alumina crucible for 2 h. The completion of reaction and the formation of desired compounds were checked by X-ray diffraction technique.

The XRD data were obtained on sintered pellets of NN and NT with an X-ray diffractometer (Rikagu Miniflex, Japan) at room temperature, using  $\text{CuK}_\alpha$  radiation ( $\lambda = 1.5405 \text{ \AA}$ ). The scanning ( $2\theta$ ) was performed from  $20^\circ$ - $70^\circ$  with a step of  $0.04^\circ$  at a scanning rate of  $2.0^\circ/\text{min}$ . The  $2\theta$  vs. intensity data were plotted with the WinPLOT program and the angular positions of the peaks were obtained with the same program (Roisnel and Rodriguez-Carvajal 2000). The dimensions of the unit cell,  $hkl$  values and space group of both the compounds were obtained using the DICVOL program in the FullProf 2012 software and then refinements were carried out through the profile matching routine of FullProf (Rodriguez-Carvajal 2012). The Bragg peaks were modeled with pseudo-Voigt function and the background was estimated by linear interpolation between selected background points. The Fourier Transformed Infrared (FTIR) spectra of NN and NT samples along with their constituent compounds were collected in the transmission mode using an Alpha-T Bruker FTIR spectrophotometer in the range of  $500$ - $4500 \text{ cm}^{-1}$ . The electrical measurements were carried out on a symmetrical cell of type  $\text{Ag}|\text{Ceramic}|\text{Ag}$ , where Ag is a conductive paint coated on either side of the pellets. Electrical impedance ( $Z$ ), phase angle ( $\theta$ ), loss tangent ( $\tan\delta$ ) and capacitance ( $C$ ) were measured as function of frequency ( $0.1 \text{ kHz}$ - $1 \text{ MHz}$ ) at different temperatures ( $35^\circ\text{C}$ - $500^\circ\text{C}$ ) using a computer-controlled LCR Hi-Tester (HIOKI 3532-50, Japan) interfaced with a microprocessor controlled dry temperature controller (DPI-1100, Sartech Intl., India) at a heating rate of  $4^\circ\text{C}/\text{min}$ . AC conductivity data were thus obtained using the relation:  $\sigma_{ac} = 2\pi f \varepsilon_0 \varepsilon \tan\delta$  where  $f$ ,  $\varepsilon$ , and  $\tan\delta$  are operating frequency, dielectric constant and loss tangent respectively.

## 3. Results and discussion

X-ray diffraction patterns of NN and NT along with their Rietveld refinement profiles are shown in Fig. 1. It can be seen that the observed and calculated XRD profiles for both the compounds are in fair agreement, suggesting the formation of single phase compounds having orthorhombic structure with space group  $Pnmm(47)$ . The crystal data and refinement factors of

Table 1 The crystal data and refinement factors of NaNbO<sub>3</sub> and NaTaO<sub>3</sub> obtained from X-ray powder diffraction data

| Parameters                 | NaNbO <sub>3</sub> | NaTaO <sub>3</sub> |
|----------------------------|--------------------|--------------------|
| Crystal System             | Orthorhombic       | Orthorhombic       |
| Space group(No.)           | <i>Pmmm</i> (47)   | <i>Pmmm</i> (47)   |
| <i>a</i> (Å)               | 5.5659             | 5.5262             |
| <i>b</i> (Å)               | 5.5071             | 5.4812             |
| <i>c</i> (Å)               | 3.8792             | 3.8961             |
| <i>V</i> (Å <sup>3</sup> ) | 118.9057           | 118.0126           |
| <i>R<sub>p</sub></i>       | 25.6               | 34.6               |
| <i>R<sub>wp</sub></i>      | 22.3               | 33.1               |
| <i>R<sub>exp</sub></i>     | 10.5               | 9.66               |
| <i>R<sub>B</sub></i>       | 0.219              | 0.358              |
| <i>R<sub>F</sub></i>       | 0.133              | 0.451              |
| $\chi^2$                   | 4.499              | 11.7               |
| <i>d</i>                   | 1.2964             | 1.6524             |
| <i>Q<sub>D</sub></i>       | 1.8378             | 1.8392             |
| <i>S</i>                   | 2.123              | 3.427              |

### Description of parameters

*R<sub>p</sub>* (profile factor) =  $100[\sum|y_i - y_{ic}|/\sum|y_i|]$ , where *y<sub>i</sub>* is the observed intensity and *y<sub>ic</sub>* is the calculated intensity at the *i*<sup>th</sup> step.

*R<sub>wp</sub>* (weighted profile factor) =  $100[\sum\omega_i|y_i - y_{ic}|^2/\sum\omega_i(y_i)^2]^{1/2}$ , where  $\omega_i = 1/\sigma_i^2$  and  $\sigma_i^2$  is variance of the observation.

*R<sub>exp</sub>* (expected weighted profile factor) =  $100[(n-p)/\sum\omega_i(y_i)^2]^{1/2}$ , where *n* and *p* are the number of profile points and refined parameters, respectively.

*R<sub>B</sub>* (Bragg factor) =  $100[\sum|I_{obs} - I_{calc}|/\sum|I_{obs}|]$ , where *I<sub>obs</sub>* is the observed integrated intensity and *I<sub>calc</sub>* is the calculated integrated intensity.

*R<sub>F</sub>* (crystallographic *R<sub>F</sub>* factor) =  $100[\sum|F_{obs} - F_{calc}|/\sum|F_{obs}|]$ , where *F* is the structure factor,  $F = \sqrt{I/L}$ , where *L* is Lorentz polarization factor.

$\chi^2 = \sum\omega_i(y_i - y_{ic})^2$ .

*d* (Durbin–Watson statistics) =  $\sum\{[\omega_i(y_i - y_{ic}) - \omega_{i-1}(y_{i-1} - y_{i-1c})]^2\}/\sum[\omega_i(y_i - y_{ic})]^2$ .

*Q<sub>D</sub>* = expected *d*.

*S* (goodness of fit) = (*R<sub>wp</sub>*/*R<sub>exp</sub>*).

both NN and NT, obtained from XRD data, are depicted in Table 1. This result is in consistent with the similar system (Taub *et al.* 2013, Sindhu *et al.* 2012, Zhao *et al.* 2012). A little difference in the unit cell parameters as well as unit cell volume of NN and NT were observed, which may be due to the difference in the ionic radii of Nb<sup>5+</sup> (0.78 Å) and Ta<sup>5+</sup> (0.64 Å) ions.

Fig. 2 shows the FTIR spectra of the perovskites (a) NaNbO<sub>3</sub> and (b) NaTaO<sub>3</sub> along with the constituent carbonate (Na<sub>2</sub>CO<sub>3</sub>) and oxides (Nb<sub>2</sub>O<sub>5</sub>/Ta<sub>2</sub>O<sub>5</sub>). The IR spectra of the Na<sub>2</sub>CO<sub>3</sub> comprises of a weak band at 686 cm<sup>-1</sup> which corresponds to in plane CO<sub>3</sub><sup>2-</sup> bending, a relatively strong band at 866 cm<sup>-1</sup> which corresponds to out of plane CO<sub>3</sub><sup>2-</sup> bending along with a very weak band and an intense peak at 1068 cm<sup>-1</sup> and at 1409 cm<sup>-1</sup> which corresponds to C-O symmetric stretching. The bands at 1639 cm<sup>-1</sup> and 3443 cm<sup>-1</sup> are assigned to the bending of O-H-O and O-H stretching modes of vibration due to physically adsorbed water molecules on the surface of the sample during palletisation with KBr. Further, in case of Nb<sub>2</sub>O<sub>5</sub> two broad bands at 620 cm<sup>-1</sup> and

828  $\text{cm}^{-1}$  are observed which are assigned to stretching modes of Nb-O and Nb=O vibrations (Rojac *et al.* 2012, Mathai *et al.* 2012). Also, the FTIR spectrum of  $\text{Ta}_2\text{O}_5$  the metal oxide (Ta-O) bonds ranges in the lower frequency region of 600  $\text{cm}^{-1}$  to 760  $\text{cm}^{-1}$  can easily be seen. With the exception of slight variation in the position, the peaks of the starting carbonates and oxides are consistent with the vibrations characteristic of  $\text{CO}_3^{2-}$ , Me-O and Me=O and are in agreement with the literature data (Rojac *et al.* 2012). Furthermore, the peaks within the range 500  $\text{cm}^{-1}$  to 900  $\text{cm}^{-1}$  of the starting oxides and carbonates are not present in the product compounds and new prominent peaks at 633  $\text{cm}^{-1}$  (in  $\text{NaNbO}_3$ ) and 557  $\text{cm}^{-1}$  and 672  $\text{cm}^{-1}$  (in  $\text{NaTaO}_3$ ) can be observed which corresponds to the Nb-O and Ta-O bonds thereby confirming the formation of desired compound (Rojac *et al.* 2012). Both the samples under investigation contain the multiple peaks (A-O absorption bands) in the frequency region 1000-1640  $\text{cm}^{-1}$ , which are due to the presence of Na-O vibrations. Further, IR spectra are very sensitive to the presence of moisture during the course of experimentation. A broad and strong peak can easily be seen around 3400-3500  $\text{cm}^{-1}$  which are due to free water molecules ( $\text{H}_2\text{O}$  bands) and strong stretching (antisymmetric and symmetric) modes of the OH-group (Jha and Prasad 2012, Kumar *et al.* 2013).

The temperature dependence of dielectric constant ( $\epsilon$ ) and loss tangent ( $\tan\delta$ ) at different frequencies for NN and NT are shown in Fig. 3. The plots for both the compounds show diffuse

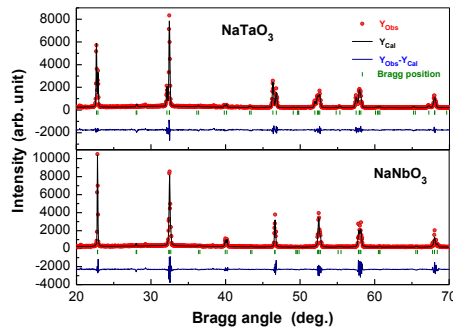


Fig. 1 Rietveld refined patterns of  $\text{NaNbO}_3$  and  $\text{NaTaO}_3$ . Symbols represent the observed data points and the solid lines their Rietveld fit

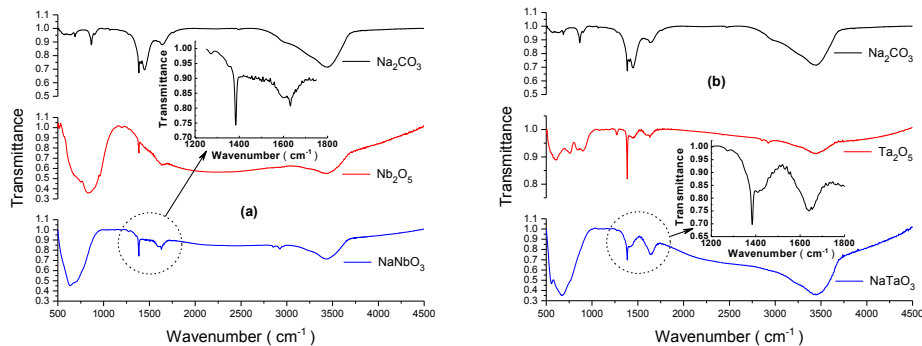


Fig. 2 FTIR spectra for (a)  $\text{NaNbO}_3$  and (b)  $\text{NaTaO}_3$  ceramics along with their constituent compounds

phase transition (DPT)  $T_m$ , respectively, at 394°C ( $\epsilon_m = 578$ ) and 430°C ( $\epsilon_m = 395$ ). Similar results have been found by Koruza *et al.* (2010). Also, the maximum value of  $\epsilon$  decreases and  $\epsilon$ - $T$  curves flatten with the increase in frequency. The broadening in the dielectric peak is a common occurrence in such type of materials. The multiple ion occupation at different sites, microstructure and sintering process causes deviation from normal Curie-Weiss behaviour, where  $T_m$  is not sharp, but physical properties change rather gradually over a temperature range, and is known as DPT. The DPT can be explained by modified Curie-Weiss law:  $1/\epsilon - 1/\epsilon_{\max} = A(T - T_C)^\gamma$ , where  $\gamma$  is called the diffusivity parameter giving the measure of broadness in phase transition and normally varies between 1 and 2 (Prasad *et al.* 1996). The values of  $\gamma$  are estimated to be 1.27 and 1.89, respectively for NN and NT using the method of least squares, which confirms DPT. The values of  $\epsilon$  and  $\tan\delta$  at room temperature are, respectively, found to be 105 and 0.093 for NN and 211 and 0.21 and NT at 1 kHz.

Fig. 4 shows the log-log plots of ac electrical conductivity versus frequency at different temperatures. The ac conductivity spectrum for both NN and NT shows dispersion throughout the chosen frequency range and with the increment in temperature plots get flattened (plateau value). The switch from the frequency-independent to the dependent regions shows the onset of the conductivity relaxation phenomenon which indicates the translation from long range hopping to the short range ion-motion (Mizaras *et al.* 1997). This observation can be well expressed by the Jonscher's universal power law:  $\sigma_{ac} = \sigma_{dc} + A\omega^s$ , where  $\sigma_{dc}$  is the frequency independent (dc) part of conductivity (Jonscher 1983). The second term in the right hand side is the frequency sensitive region with  $0 \leq s \leq 1$ . It was found that the value of index  $s$  decreases with the rise of temperature and is always less than 1. The model based on hopping of charge carriers  $s = 1 - 6k_B T / \{W_M - k_B T \ln(1/\omega\tau_0)\}$ , where,  $W_M$  is the energy required to cross the barrier height, which predicts a decrease in the value of the index 's' with the increase in temperature and so found to be consistent with the experimental results. Therefore, the conduction in both the systems could be considered due to the short-range translational type hopping of charge carriers (AmarNath and Prasad 2012).

It is observed that the hopping conduction mechanism is generally consistent with the

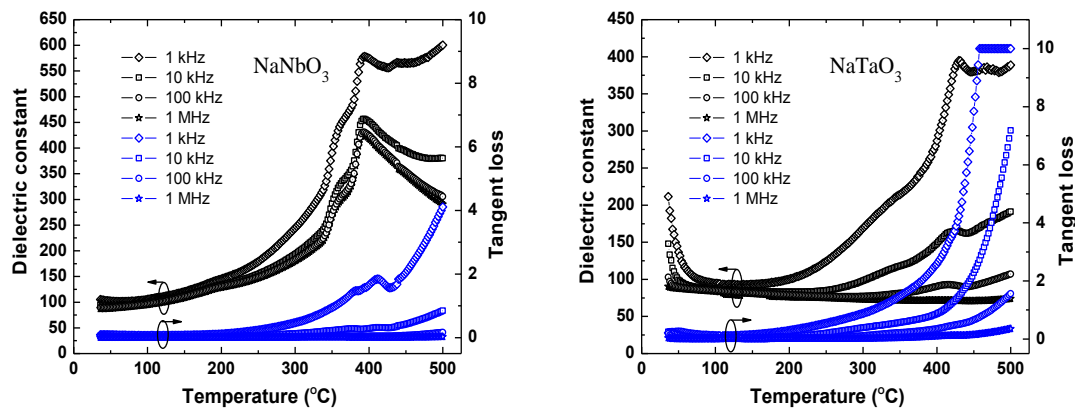


Fig. 3 Temperature dependence of dielectric constant and tangent loss of NaNbO<sub>3</sub> and NaTaO<sub>3</sub> at different frequencies

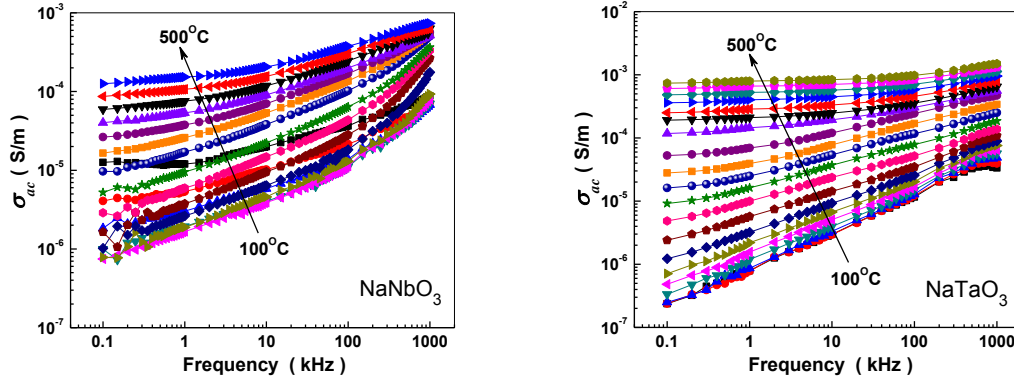


Fig. 4 Frequency dependence of ac conductivity of  $\text{NaNbO}_3$  and  $\text{NaTaO}_3$  at different temperatures

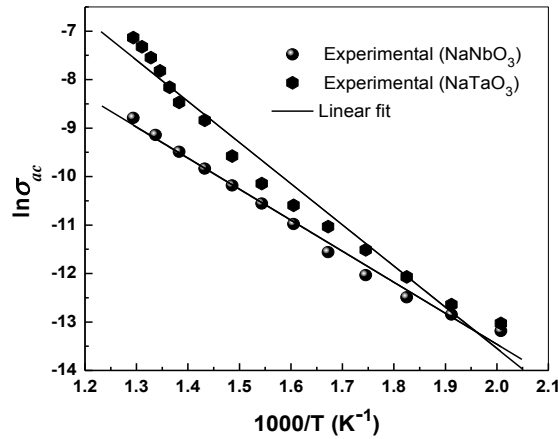


Fig. 5 Temperature dependence of ac conductivity of  $\text{NaNbO}_3$  and  $\text{NaTaO}_3$  at 1 kHz

existence of a high density of states in the materials having band gap like that of semiconductor. Due to localization of charge carriers, formation of polarons takes place and the hopping conduction may occur between the nearest neighboring sites. Fig. 5 shows the variation of ac conductivity versus  $10^3/T$  for NN and NT. The nature of variation is almost linear indicating the ohmic nature of contact and conductivity obeys the Arrhenius relationship:  $\sigma_{ac} = \sigma_o + \exp(-E_a/k_B T)$ , where  $E_a$  is the apparent activation energy of conduction,  $k_B$  is the Boltzmann constant and  $T$  is the absolute temperature. The nature of variation shows the negative temperature coefficient of resistance (NTCR) behaviour in NN and NT. The values of  $E_a$  for NN and NT are estimated, respectively, to be 0.40 eV and 0.53 eV at 1 kHz using a linear least square fitting. The low value of  $E_a$  may be due to the carrier transport through hopping between localized states in a disordered manner (Prasad *et al.* 2006, AmarNath and Prasad 2012).

#### 4. Conclusions

Polycrystalline samples of NaNbO<sub>3</sub> and NaTaO<sub>3</sub>, prepared through a high temperature solid state reaction route, were found to possess perovskite type orthorhombic structure with the space group *Pmmm*(47). Dielectric studies showed the diffuse phase transition at 394°C for NN and 430°C for NT. It is observed that ac conductivity exhibits Jonscher's power law and the carrier transport follows hopping type conduction mechanism in both the compounds.

#### References

- AmarNath, K. and Prasad, K. (2012), "Structural and electric properties of perovskite Ba(Sm<sub>1/2</sub>Nb<sub>1/2</sub>)O<sub>3</sub>-BaTiO<sub>3</sub> ceramic", *Adv. Mater. Res.*, **1**(2), 115-128.
- Bhagat, S., AmarNath, K., Chandra, K.P., Singh, R.K., Kulkarni, A.R. and Prasad, K. (2013), "The structural, electrical and magnetic properties of perovskite (1-x)Ba(Fe<sub>1/2</sub>Nb<sub>1/2</sub>)O<sub>3</sub>-xBaTiO<sub>3</sub> ceramics", *Adv. Mater. Lett.*, in press.
- Chen, X.M., Lu, Y.T., Jin, D.Z. and Liu, X.Q. (2005), "Dielectric and ferroelectric characterization of Na(Ta,Nb)O<sub>3</sub> solid solution ceramics", *J. Electroceram.*, **15**(1), 21-26.
- Damjanovic, D., Klein, N., Li, J. and Porokhonsky, V. (2010), "What can be expected from lead-free piezoelectric materials?", *Funct. Mater. Lett.*, **3**(1), 5-13.
- Du, H., Huang, Y., Tang, H., Qin, H. and Feng, W. (2013a), "Dielectric and piezoelectric properties of SrZrO<sub>3</sub>-modified (K<sub>0.45</sub>Na<sub>0.51</sub>Li<sub>0.04</sub>)(Nb<sub>0.90</sub>Ta<sub>0.04</sub>Sb<sub>0.06</sub>)O<sub>3</sub> lead-free piezoceramics", *Mater. Lett.*, **106**, 141-144.
- Du, H., Huang, Y., Tang, H., Feng, W., Qin, H. and Lu, X. (2013b), "Structure and electrical properties of [(K<sub>0.49</sub>Na<sub>0.51</sub>)<sub>1-x</sub>Li<sub>x</sub>](Nb<sub>0.90</sub>Ta<sub>0.04</sub>Sb<sub>0.06</sub>)O<sub>3</sub> lead-free piezoceramics", *Ceram. Int.*, **39**, 5689-5694.
- Eichel, R.A. and Kungl, H. (2010), "Recent developments and future perspectives of lead-free ferroelectrics", *Funct. Mater. Lett.*, **3**(1), 1-4.
- Hsiao, Y.J., Chang, Y.H., Chang, Y.S., Fang, T.H., Chai, Y.L., Chen, G.J. and Huang, T.W. (2007), "Growth and characterization of NaNbO<sub>3</sub> synthesized using reaction-sintering method", *Mater. Sci. Engg. B*, **136**(2-3), 129-133.
- Jha, A.K. and Prasad, K. (2012), "Biological synthesis of cobalt ferrite nanoparticles", *Nanotechnol. Dev.*, **2:e9**, 46-51.
- Jonscher, A.K. (1983), *Dielectric Relaxation in Solids*, Chelsea, New York.
- Kennedy, B.J., Prodjosantoso, A.K. and Howard, C.J. (1999), "Powder neutron diffraction study of the high temperature phase transitions in NaTaO<sub>3</sub>", *J. Phys.: Condens. Matter*, **11**(33), 6319-6328.
- Koruza, J., Tellier, J., Malič, B., Bobnar, V. and Kosec, M. (2010), "Phase transitions of sodium niobate powder and ceramics, prepared by solid state synthesis", *J. Appl. Phys.*, **108**(11), 113509-113518.
- Kumar, S., Sahay, L.K., Jha, A.K. and Prasad, K. (2013), "Synthesis of (Ag<sub>0.5</sub>Fe<sub>0.5</sub>)TiO<sub>3</sub> nanocrystalline powders using stearic acid gel method", *Adv. Mater. Lett.*, **4**(2), in press.
- Kumari, K., Prasad, A. and Prasad K. (2011), "Structural and dielectric properties of ZnO added (Na<sub>1/2</sub>Bi<sub>1/2</sub>)TiO<sub>3</sub> ceramic", *J. Mater. Sci. Technol.*, **27**(3), 213-217.
- Mathai, S.K., Vidya, S., Solomon, S. and Thomas, J.K. (2012), "A study of dielectric and optical properties of crystalline Nb<sub>2</sub>O<sub>5</sub> nanoparticles synthesized by a modified combustion technique", *Int. J. Appl. Math. Sci.*, **5**(1), 19-34.
- Mizaras, R., Takashige, M., Banys, J., Kojima, S., Grigas, J., Hamazaki S.I. and Brilingas, A. (1997), "Dielectric relaxation in Ba<sub>2</sub>NaNb<sub>5(1-x)</sub>Ta<sub>5x</sub>O<sub>15</sub> single crystals", *J. Phys. Soc. Jpn.*, **66**, 2881-2885.
- Panda, P.K. (2009), "Review: environmental friendly lead-free piezoelectric materials", *J. Mater. Sci.*, **44**(19), 5049-5062.
- Prasad, K., Choudhary, R.N.P., Choudhary, S.N. and Sati, R. (1996), "On the structural and electrical

- properties of modified  $\text{PbTiO}_3$  ceramics”, *Bull. Mater. Sci.*, **19**(3), 505-512.
- Prasad, K., Suman, C.K. and Choudhary, R.N.P. (2006), “Electrical characterization of  $\text{Pb}_2\text{Bi}_3\text{SmTi}_5\text{O}_{18}$  ceramic using impedance spectroscopy”, *Adv. Appl. Ceram.*, **105**, 258-264.
- Reznitchenko, L.A., Turik, A.V., Kuznetsova, E.M. and Sakhnenko, V.P. (2001), “Piezoelectricity in  $\text{NaNbO}_3$  ceramics”, *J. Phys.: Condens. Matter*, **13**(17), 3875-3882.
- Rödel, J., Jo, W., Seifert, K.T.P., Anton, E.M., Granzow, T. and Damjanovic, D. (2009), “Perspective on the development of lead-free piezoceramics”, *J. Am. Ceram. Soc.*, **92**(6), 1153-1177.
- Rodriguez-Carvajal, J., “FullProf 2000: A Rietveld refinement and pattern matching analysis program”, (Version: February 2012), Laboratoire Léon Brillouin (CEA-CNRS), France.
- Roissnel, J. and Rodriguez-Carvajal, J. (2000), WinPLOTR, Laboratoire Léon Brillouin (CEA-CNRS) Centre d’Etudes de Saclay: Gif sur Yvette Cedex, France.
- Rojac, T., Šegedin, P. and Kosec, M. (2012), Using infrared spectroscopy to identify new amorphous phases - A case study of carbonato complex formed by mechanochemical processing, book edited by Theophile Theophanides.
- Seo, I.T., Choi, C.H., Song, D., Jang, M.S., Kim, B.Y., Nahm, S., Kim, Y.S., Sung, T.H. and Song, H.C. (2013), “Piezoelectric properties of lead-free piezoelectric ceramics and their energy harvester characteristics”, *J. Am. Ceram. Soc.*, **96**(4), 1024-1028.
- Shrout, T.R. and Zhang, S.J. (2007), “Lead-free piezoelectric ceramics: Alternatives for PZT?”, *J. Electroceram.*, **19**(1), 111-124.
- Sindhu, M., Ahlawat, N., Sanghi, S., Agarwal, A., Kumari, A.R. and Ahlawat, N.N. (2012), “Rietveld refinement and dc conductivity of  $\text{Na}_{0.5}\text{K}_{0.5}\text{NbO}_3$  ceramics”, *Adv. Mater. Res.*, **585**, 210-213.
- Takenaka, T. and Nagata, H. (2005), “Current status and prospects of lead-free piezoelectric ceramics”, *J. Euro. Ceram. Soc.*, **25**(12), 2693-2700.
- Taub, J., Ramajo, L. and Castro, M.S. (2013), “Phase structure and piezoelectric properties of Ca- and Ba-doped  $\text{K}_{1/2}\text{Na}_{1/2}\text{NbO}_3$  lead-free ceramics”, *Ceram. Int.*, **39**, 3555-3561.
- Vendrell, X., García, J.E., Rubio-Marcos, F., Ochoa, D.A., Mestres, L. and Fernández, J.F. (2013), “Exploring different sintering atmospheres to reduce nonlinear response of modified KNN piezoceramics”, *J. Euro. Ceram. Soc.*, **33**, 825-831.
- Wunderlich, W. (2009), “ $\text{NaTaO}_3$  composite ceramics – A new thermoelectric material for energy generation”, *J. Nuclear Mater.*, **389**, 57-61.
- Zhao, Y., Huang, R., Liu, R. and Zhou, H. (2012), “Phase structure of  $\text{Li}_{0.058}(\text{Na}_{0.51}\text{K}_{0.49})_{0.942}\text{NbO}_3$  lead-free piezoelectric ceramics”, *Mater. Lett.*, **84**, 52-55.